

# Local contact inhibition leads to universal principles of cell population growth

GREGORY J. KIMMEL<sup>1</sup>, JEFFREY WEST<sup>1</sup>, MEHDI DAMAGHI<sup>2</sup>, ALEXANDER R. A.  
ANDERSON<sup>1</sup>, AND PHILIPP M. ALTROCK<sup>1,3,\*</sup>

<sup>1</sup>*Department of Integrated Mathematical Oncology, H. Lee Moffitt Cancer Center and Research  
Institute, Tampa, FL 33612, USA*

<sup>2</sup>*Department of Cancer Physiology, H. Lee Moffitt Cancer Center and Research Institute, Tampa, FL  
33612, USA*

<sup>3</sup>*Department of Evolutionary Theory, Max Planck Institute for Evolutionary Biology, 24306 Ploen,  
Germany*

*\* Corresponding author: philipp.altrock@gmail.com*

August 24, 2021

## Abstract

Cancer cell population dynamics often exhibit remarkably replicable, universal laws despite their underlying heterogeneity. Mechanistic explanations of universal cell population growth remain partly unresolved to this day, whereby population feedback between the microscopic and mesoscopic configurations can lead to macroscopic growth laws. We here present a unification under density-dependent birth events via contact inhibition. We consider five classical tumor growth laws: exponential, generalized logistic, Gompertz, radial growth, and fractal growth, which can be seen as manifestations of a single microscopic model. Our theory is substantiated by agent based simulations and can explain growth curve differences in experimental data from *in vitro* cancer cell population growth. Thus, our framework offers a possible explanation for the large number of mean-field laws that can adequately capture seemingly unrelated cancer or microbial growth dynamics.

**Keywords:** population growth, cancer growth curves, cell motility, contact inhibition

# 1 Introduction

Cancer cell population dynamics often exhibit remarkably replicable, universal laws (Wodarz and Komarova, 2005; Pérez-García et al., 2020) despite their genetic, epigenetic, and phenotypic heterogeneity (Reiter et al., 2019; Hausser and Alon, 2020). The derivation of a universal growth law for tumors has been the subject of investigations for decades (Mombach et al., 2002; Guiot et al., 2003; Rodriguez-Brenes et al., 2013; Benzekry et al., 2014). The winding search for a comprehensive mathematical characterization of tumor growth has belied two seemingly opposing concepts. First, a growth model should accurately describe the empirical data (Altrock et al., 2015; Brady and Enderling, 2019). Second, a growth model should be based on and derived from a biological mechanistic framework (Cheng et al., 2009; Gerlee, 2013; West and Newton, 2019). Cell population growth models with underlying mechanisms should be preferred because of their utility in comparative studies, model selection, and hypothesis generation.

Models with a strong biological motivation often receive less attention due to their lack of data-fitting potential, and mechanistic approaches might be preferably used (Gerlee, 2013). Exponential growth often fits well to data, but dynamics over longer timescales are better approximated by logistic, Gompertz, or power law models (Benzekry et al., 2014). Intriguingly, the Gompertz model was originally employed as the best match to observed exponential decay of net cancer growth rates (Laird, 1964). Attempts at mechanistic explanations of growth with time-dependent rates remain partly unresolved to this day.

Gompertzian models find wide application, e.g. in finance (Islam et al., 2002), population re-growth through niche occupation (Kimmel et al., 2021), microbial dynamics (Zwietering et al., 1990), and tumors (Steel, 1977a; Spratt et al., 1993). Its use in cancer modeling, even without biological mechanistic foundation, is indicative of its predictive and descriptive potential (Benzekry et al., 2014). To reconcile the disconnect between descriptive power and mechanistic insight, several studies have proposed a deeper understanding. Recent work by West & Newton derives several related growth laws mechanistically by assuming gradual occupation of cellular microstates (West and Newton, 2019; West et al., 2016). This approach indicates that population feedback between the populations’s microscopic and mesoscopic configurations can lead to macroscopic growth laws.

In cancer cells, increased motility allows for continued movement after contact with neighbors (Ribatti, 2017). In normal tissues, high cell density leads to inhibition of cellular proliferation upon reaching maximal capacity (Eagle and Levine, 1967; Pavel et al., 2018). Loss of contact inhibition is common in solid tumors and increases invasion (Mayor and Carmona-Fontaine,

2010; McClatchey and Yap, 2012). Cell density is also impacted by cell migration. There is often assumed to be a dichotomy between migration (go) and proliferation (grow) (Hatzikirou et al., 2012; Gallaher and Anderson, 2013; Kimmel et al., 2020)). The go-or-grow hypothesis remains controversial (Vittadello et al., 2020), yet might also arise from DNA replication and genomic instability (Aguilera and Gómez-González, 2008; Kimmel et al., 2020).

Here, we present a unifying framework that leads to multiple classical growth laws based on the mechanism of local contact inhibition. Three major factors regulate contact inhibition and tumor cell density dynamics: proliferation, migration, and the size of the local interaction region. Each of these microscopic factors may be subject to heterogeneity and temporal variations. Inevitably, these variations lead to diverse macroscopic growth dynamics. Key properties of these macroscopic dynamics could still be explained using simple bio-physical mechanisms. The theory we introduce here considers five classical tumor growth laws: exponential, generalized logistic, Gompertz, radial growth, fractal growth. Corroborated with agent based simulations and statistical analysis of data from *in vitro* cancer cell population growth experiments, we show that these five growth laws are manifestations of a single microscopic model under varied assumptions of contact inhibition.

## 2 Methods

Here, we describe the experimental (*in vitro*) procedures, analytical modeling, and computational (agent based) modeling, and data fitting procedures. The quantities and parameters of the model are summarized in Table 1.

### 2.1 Cell culture and immunofluorescence experiments

For cancer cell culture experiments, we used the MCF-7, MDA-mb-231 breast cancer cell lines (Figure 1), as well as ovarian cancer cell lines OVCA3, A2780s, TOV112D, which were acquired from American Type Culture Collection (ATCC, Manassas, VA, 2007-2010) and were maintained in RPMI 1640 (Life Technologies, Cat# 11875-093) supplemented with 10% fetal bovine serum (HyClone Laboratories). Cells were tested for mycoplasma contamination and authenticated using short tandem repeat DNA typing according to ATCC guidelines.

Cells were seeded on an 8 chamber microscopy slide overnight. They were then rinsed with phosphate-buffered saline (PBS), fixed in cold Methanol:Acetone (1:1) for 10 minutes and fur-

Parameter name	Symbol	Typical values	Range
Number of cells at time $t$	$n(t)$	$0, \dots, 10^8$	$[0, \infty)$
System domain length	$L$	$100, \dots, 1000$	$[0, \infty)$
Birth neighborhood domain/set for cell $i$	$\Omega_i$	–	–
Birth neighborhood size for cell $i$	$\omega_i$	$4, \dots, 8$	$[0, 24)$
Mean birth neighborhood	$\mu_\omega$	$4, \dots, 8$	$[0, 24)$
Density-dependent birth rate at site $i$ with population size $n$	$\lambda_{i,n}$	–	–
Density-dependent death rate at site $i$ with population size $n$	$\delta_{i,n}$	–	–
Cell motility coefficient	$\Gamma$	$0, \dots, \infty$	$[0, \infty)$
Cell migration rate (ABM)	$m$	$0, \dots, 1$	$[0, \infty)$
Migration neighborhood set (ABM)	$\Phi$	–	–
Migration neighborhood size (ABM)	$\phi$	$4, \dots, 8$	$[0, \infty)$

**Table 1.** Parameter table.

ther permeabilized by 0.5% triton 100 and then blocked with 5% bovine serum albumin in PBS. Samples were incubated with LAMP2 rabbit primary antibody (1:100; ab 218529) from abcam and secondary Alexa-Fluor 488 antirabbit (1:1000) antibody. WGA was used to stain the membrane and DAPI for the Nucleous. Coverslips were mounted using ProLong Gold Antifade Reagent (Life Technologies) and images were captured with a Leica TCS SP5 (Leica) confocal microscope. Cell count measurements were performed with an oil-immersion x63 objective.

## 2.2 Agent based simulations of tumor growth

Simulations of a stochastic agent based model were performed using the Hybrid Automata Library software package, which allows for fast simulation of tumor growth models in spatial domains with real-time visualization. The model is implemented using Java JDK Version 8. Each stochastic simulation is initialized with a single tumor cell placed in the center of an  $L \times L$  two-dimensional domain. The model is a birth-death-migration process, carried out on a two-dimensional lattice where each grid point contains at most one single tumor cell. In each generation, all cells in the domain follow the birth-death-migration cell step flowchart (Figure 2A). While iterating through all cells, the current focal cell may migrate to a random neighboring

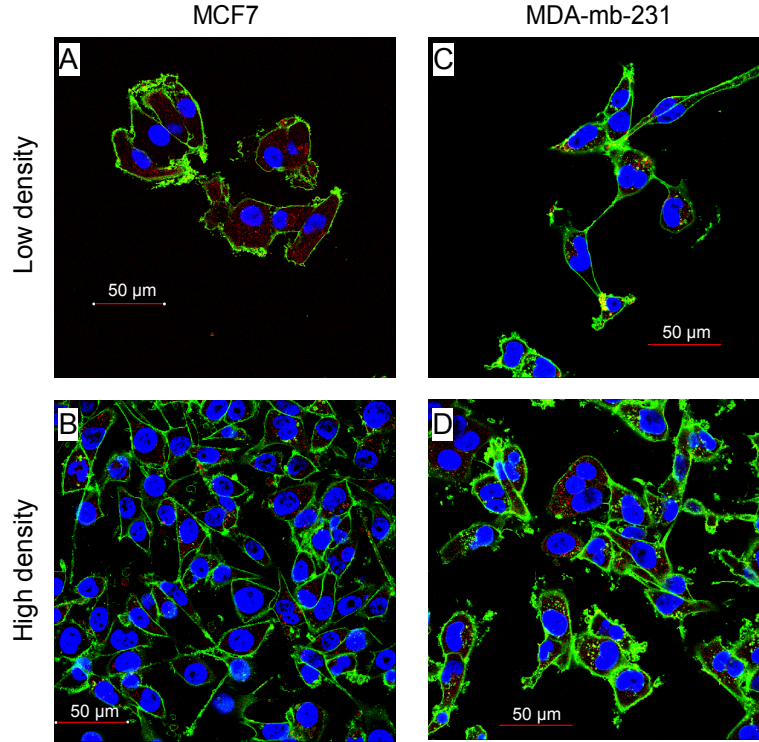


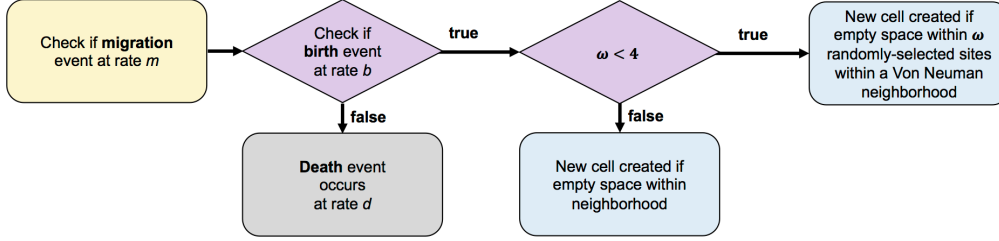
**Figure 1.** Experimental observations of cancer cells distributed at low and high density. **A, B:** Breast cancer cell line MCF-7 at low and high density. **C, D:** Breast cancer cell line MDA-mb-231 at low and high density.

grid point at rate  $m$ . The migration neighborhood is a precisely defined set of lattice locations defined in relation to the focal cell's location, defined as  $\Phi = 1, 2, \dots, \phi$  ( $\phi \in L \times L$ ) with example neighborhoods given in Figure 2B. Next, the focal cell undergoes division at a rate  $b$ , where the daughter cell is placed in a random neighboring grid point and the parent cell remains on the original lattice point. Similarly, the lattice locations within the birth neighborhood are precisely defined as  $\Omega = 1, 2, \dots, \omega$ , which may be identical, larger, or smaller than  $\Phi$ . If a birth event does not occur, the cell may undergo apoptosis (death) and is removed from the domain. After each generation, the update order in which cells iterate is shuffled.

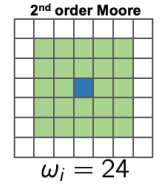
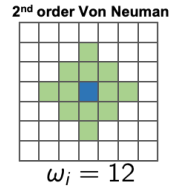
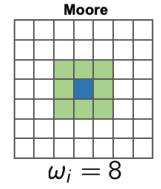
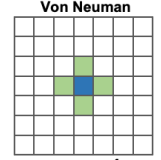
### 2.3 Analytical model of tumor growth

Let us define a location with generalized coordinates  $\vec{q}$  and suppose that the probability for finding a cell at a particular site, given  $n$  cells at time  $t$ , is given by the probability density (mass) function  $f(\vec{q}|n, t)$ . We assume a birth-death process, birth events are density-dependent.

### A. Agent-based model (ABM)



### B. Neighborhoods



### C. Theory flowchart

- $L$  = Domain
- $l$  = Domain lattice sites
- $\omega_i$  = Birth neighborhood size of focal cell  $i$
- = Birth neighborhood site
- = Prototypical focal cell with motion

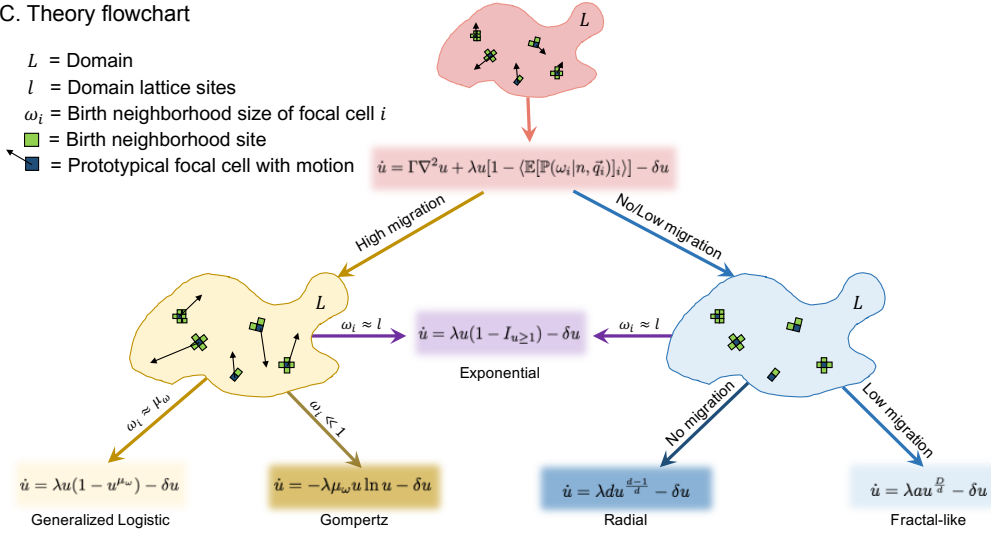


**Figure 2. Overview of computational modeling and theoretical approaches.** **A:** agent based model (ABM) cell step flowchart. At each time step, the cell checks if a migration event occurs (at rate  $m$ ). Next, the cell checks if a birth even occurs, and divides if there is a free lattice point to place the new daughter cell within the birth neighborhood. If no free space is available, a birth does not occur. In the case of no birth, the cell may undergo death (at rate  $d$ ). **B:** Prototypical neighborhood paradigms for migration or birth for the individual-based model simulations. **C:** Schematic of the theory hierarchy that describes the general model (red) and the limiting regimes we consider. High migration ( $\Gamma$  large) leads to well-mixed behavior, while low migration ( $\Gamma$  small) leads to radial growth.

An example setup is shown in in Figure 2A. Tumor growth is constrained to a two-dimensional lattice where each lattice point can contain at most a single cell.

Contact inhibition may occur within some localized region, or “neighborhood,” near a cell. Commonly used neighborhoods are shown in Figure 2B, but we can consider a neighborhood domain of any arbitrary size. The neighbor domain for the  $i^{\text{th}}$  cell we denote by  $\Omega_i$  with number of elements  $\omega_i$ . We can partition the domain into two disjoint groups via the union  $\Omega_i \cup L \setminus \Omega_i$ . Define the random variable  $X_i \in \{0, 1, \dots, \omega_i\}$  as the number of filled neighbor sites seen by cell  $i$  and let  $\mathbb{P}(X_i = x)$  be the probability of observing  $x$  filled sites. In a similar way, we will define  $Y_i \in \{0, 1, \dots, l - \omega_i - 1\}$  as the number of filled sites not in the neighborhood. In what follows, we often remove the subscripts for brevity.

Given a focal cell  $C$  at position  $\vec{q}_i$ , denoted by  $C(\vec{q}_i)$ , we seek the probability of observing  $x$  neighbors and  $y$  non-neighbors given  $n$  cells. Formally, we want an expression for the following conditional probability

$$\mathbb{P}(X_i = x, Y_i = y | n, C(\vec{q}_i)). \quad (2.1)$$

We can express the function (2.1) in terms of a product, assuming independence, to gain further insight into the behavior of this system:

$$\mathbb{P}(x, y | n, C(\vec{q}_i)) = \mathbb{P}(y | n, x, C(\vec{q}_i)) \mathbb{P}(x | n, C(\vec{q}_i)).$$

We note here that since the groups partitioned by neighborhood are disjoint, we require the condition that  $x + y = n - 1$  and so  $\mathbb{P}(y | n, x, C(\vec{q}_i)) = 1$  only if  $y = n - x - 1$  and 0 otherwise. This allows us to consider simply the conditional probability:

$$\mathbb{P}(x | n, C(\vec{q}_i)) = \frac{\mathbb{P}(x, C(\vec{q}_i) | n)}{\mathbb{P}(C(\vec{q}_i) | n)}, \quad (2.2)$$

with the restriction that  $y = n - x - 1$ . All of the information for birth is tied into this distribution. An individual-based birth-death-movement process of cell  $C(\vec{q}_i)$  with total number of cells  $n$  is defined via the following transition rates:

$$C(\vec{q}_i) \xrightarrow{\lambda_{i,n}} C(\vec{q}_i) + C(\vec{q}_j), \quad (2.3a)$$

$$C(\vec{q}_i) \xrightarrow{\delta_{i,n}} \emptyset, \quad (2.3b)$$

where  $\vec{q}_j \in \Omega_i$ . Death is density-independent (i.e. constant), while the birth rate is density-dependent through contact inhibition. That is, we only allow a birth event to occur for cell at

$\vec{q}_i$ , if a neighbor site is available:

$$\lambda_{i,n} = \lambda[1 - \mathbb{P}(\omega_i|n, \vec{q}_i)]. \quad (2.4)$$

If all cells are able to divide, we can get the population growth rate via summing over all cells. The situation in which all cells are able to divide is analogous to a well-mixed population. In contrast, we can also suppose that only a subset of the cells are able to divide. A well-known example would be a radially growing tumor where only surface-dwelling cells are able to divide. We will look at both of these cases and see how they impact the resulting growth laws.

Summing over all cells, we have the population birth and death rates given by:

$$\lambda_n = \sum_{i=1}^n \lambda_{i,n} = \lambda \sum_{i=1}^n [1 - \mathbb{P}(\omega_i|n, \vec{q}_i)], \quad (2.5a)$$

$$\delta_n = \delta n. \quad (2.5b)$$

The process governing the mean number  $\langle n \rangle$  of the birth-death process is given by

$$\frac{d\langle n \rangle}{dt} = \left\langle \lambda \sum_{i=1}^n [1 - \mathbb{P}(\omega_i|n, \vec{q}_i)] \right\rangle - \delta \langle n \rangle. \quad (2.6)$$

No approximations have been made to arrive at equation (2.6). To make a connection to more familiar growth laws, we require an approximation that is valid for large  $n$ , which allows us to replace the expectation of the product with the product of the expectations. The deterministic analog when  $n$  is large allows us to rewrite this in terms of the density  $u = \langle n \rangle/l$ :

$$\dot{u} = \Gamma \nabla^2 u + \lambda u [1 - \langle \mathbb{P}(\omega_i|n, \vec{q}_i) \rangle_i] - \delta u, \quad (2.7)$$

where we have added a migration term via diffusion. Note, the expectation,  $\mathbb{E}[\cdot]_i$  is done over each cell  $i$  and the average,  $\langle \cdot \rangle$  is the average of all possible states of  $n$  cancer cells (e.g. in this case  $n \in \{0, \dots, l\}$ ).

### 3 Results

In our analytical description, equation (2.7) presents a starting point from which multiple growth laws governed by contact inhibition at birth can be obtained. If the birth-neighborhood size is independent of  $n$  and spatial distribution  $\vec{q}$ , then (2.7) reduces to that of exponential growth.



The functional form of the growth law is highly dependent on the behavior of the average number of neighborhood sites. In the following sections, we look at special forms of  $\omega_n$  to discern some of the well-known growth laws that can emerge via contact inhibition. A schematic of the theory workflow along with sufficient conditions is shown in Figure 2C.

### 3.1 Radially expanding population

A natural starting point is to assume a growing solid tumor with no migration. Using equation (2.7) as our point of departure (with  $\Gamma = 0$ ), we assume the tumor is growing radially where only cells on the outer surface with free space have the ability to divide. Let  $r$  be the length scale for tumor cells,  $R$  be the length scale of the tumor volume and  $d$  be the dimension considered (typically  $d = 2, 3$ ). The number of tumor cells is then estimated by  $n = (R/r)^d$ . The number of cells not on the surface is given by  $n_0 = (R/r - 1)^d$ . We now write out the probability of all sites occupied explicitly,

$$\mathbb{P}(\omega_i|n, \vec{q}_i) = \begin{cases} 0 & \text{if } n = n_s, \\ 1 & \text{if } n = n_0. \end{cases} \quad (3.1)$$

Partitioning our expectation using  $n = n_s + n_0$  leads to

$$\frac{1}{n} \left[ \sum_{i=1}^{n_s} \mathbb{P}(\omega_i|n, \vec{q}_i) + \sum_{i=1}^{n_0} \mathbb{P}(\omega_i|n, \vec{q}_i) \right] = \frac{n_0}{n}. \quad (3.2)$$

Using the relations between the length scales of tumor volume versus typical cell size leads to

$$\frac{n_0}{n} = \left(1 - \frac{r}{R}\right)^d = \left(1 - n^{-1/d}\right)^d \approx \left(1 - dn^{-1/d}\right), \quad (3.3)$$

the last part, valid when  $n \gg 1$ .

The deterministic growth law is then given by

$$\frac{d\langle n \rangle}{dt} = \lambda d\langle n \rangle^{\frac{d-1}{d}} - \delta\langle n \rangle. \quad (3.4)$$

With  $d = 3$ , we obtain the Von Bertalanffy model

$$\frac{d\langle n \rangle}{dt} = 3\lambda\langle n \rangle^{\frac{2}{3}} - \delta\langle n \rangle. \quad (3.5)$$

For radial growth on a dish, we have  $d = 2$  and we obtain

$$\frac{d\langle n \rangle}{dt} = 2\lambda\langle n \rangle^{\frac{1}{2}} - \delta\langle n \rangle. \quad (3.6)$$

Thus, from a general growth equation (2.7) that includes mechanism of movement and local contact inhibition, one can derive radial cell population growth laws based on a length-scale argument.

### 3.2 Fractal growth

The notion of self-similarity has been applied to investigate tumor growth as its shape is often not a perfectly geometric object in the classic sense. Although population growth is often approximated as radial expansion, this approximation might be poor at finer length scales. Fractals and dimensionality can play a significant role in the governing laws that control tumor growth. Although these shapes are not fractals in the truest sense, as the self-similarity does not exist beyond a certain length scale (e.g. the radii of tumor cells is a natural cutoff), the principles of fractal growth can be used. In particular this idea was used to successfully show the density falling off in silica particles described in (Orbach, 1986).

The total number of cells will approximately follow  $n \propto R^d$  where  $d$  is the actual dimension of the system and  $R$  is the characteristic length scale of the growing population. In contrast, the surface dwelling cells  $n_s \propto R^D$  where  $D$  is the fractal dimension. It follows that  $n_s \propto n^{D/d}$ . This leads to a growth law

$$\frac{d\langle n \rangle}{dt} = \lambda a \langle n \rangle^{D/d} - \delta\langle n \rangle, \quad (3.7)$$

where we have introduced the constant  $a$  related to the characteristic length of the tumor cell (and to the fractal dimension of the tumor). With non-fractal growth,  $D = d - 1$  and our model reduces to that of radial growth. However, fractal growth implies a dimension  $d - 1 < D \leq d$ .

To illustrate fractal growth, we ran stochastic simulations of an individual-based model (Figure 2A) on a two-dimensional lattice, subject to varying neighborhoods (Figure 2B), and migration rates using the Hybrid Automata Library (Bravo et al., 2020). Cells may migrate at rate  $m$  within the migration neighborhood, and may undergo division at rate  $b$  within the birth neighborhood. Importantly, the birth and migration neighborhoods may be differing sizes.

Figure 3A shows tumor growth with varying neighborhood sizes. The number of surface-cells  $n_s$  is shown as a function of total size  $n$  with a snapshot of the tumor surface area after  $t = 100$

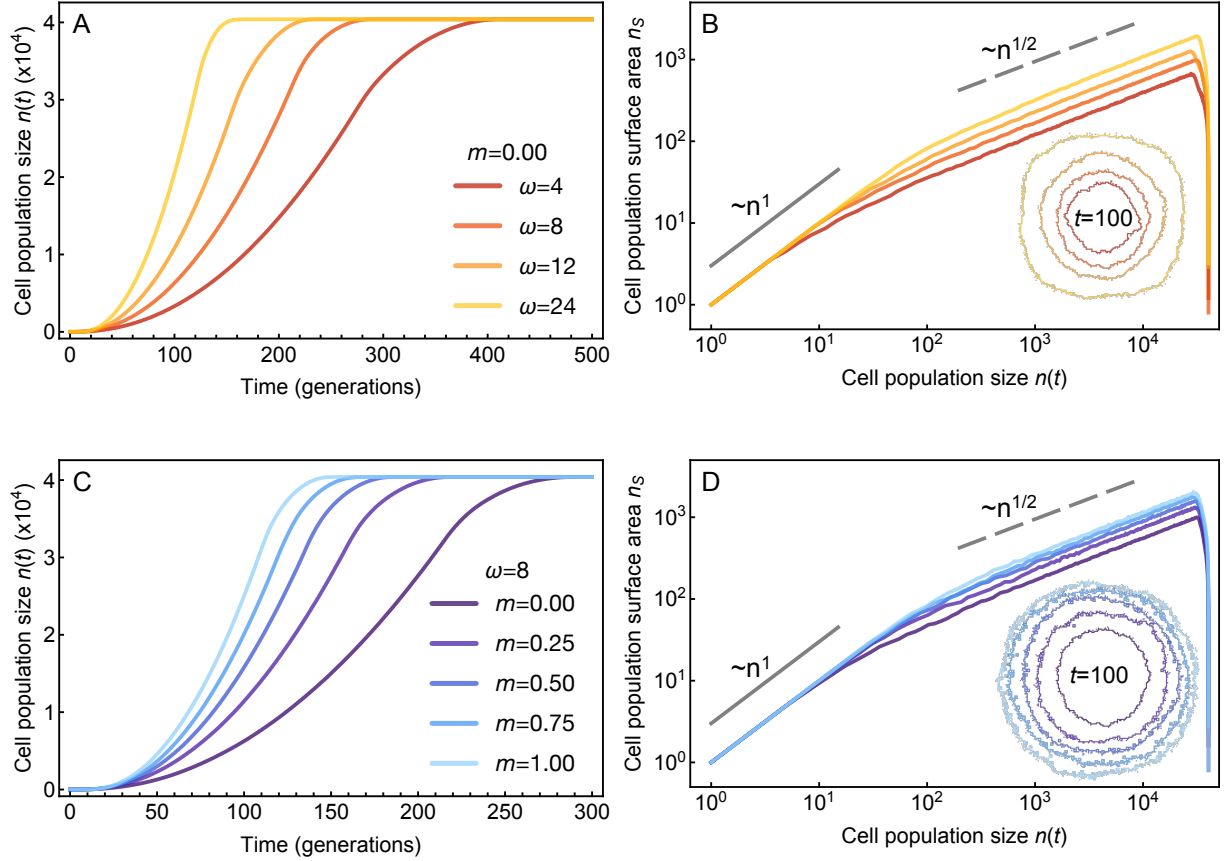


**Figure 3. Growth curves of the agent based model (ABM) depend on birth neighborhood ( $\omega$ ) and migration rate ( $m$ ).** **A:** Simulations with varied birth neighborhood size,  $\omega$ . Shown for  $201 \times 201$  domain. **B:** The cells composing the tumor surface,  $n_s$  as a function of the total population size. A large value of  $\omega$  (red) allows faster tumor growth. Large- $\omega$  tumors proliferate quickly due to increased surface area, and less contact inhibition. **C:** The same analysis for varying cell migration rate,  $m$ . **D:** Tumors with high  $m$  proliferate faster due to increased surface area. Insets (**B**, **D**) represent the tumor surface drawn at time  $t = 100$ , colored by neighborhood size,  $\omega$  and migration rate  $m$ , respectively. Note that all cells have the same birth neighborhood, thus  $\omega_i = \omega = \mu_\omega$

generations (Figure 3B). We observed a transition from a linear power law to a square root law indicating that radial growth transitions towards its characteristic growth law once the tumor reaches a certain size. Tumors with small birth neighborhoods (e.g. the Von Neumann neighborhood shown in red for  $\omega = 4$ ) remain small due to high contact inhibition of those neighborhoods. Conversely, large neighborhoods overcome contact inhibition and limited migration through increased access to free space to place daughter cells.

The effects of contact inhibition are also mitigated by increased migratory potential of tumor cells (Figure 3C-D). As the migration rate,  $m$ , increases, growth potential (Figure 3C) and surface area (Figure 3D) also increase. Here, we assume a fixed migration neighborhood (1-Moore), but in the next section we relax this assumption to explore a well-mixed assumption (i.e. a migration neighborhood which approximates the entire domain).

### 3.3 Well-mixed population growth

Let us now assume that the probability of observing  $x$  filled sites is independent of the focal cell's location  $\vec{q}$ . This approximation is justified when  $\Gamma \gg \lambda, \delta$ . Then (2.2) reduces to  $\mathbb{P}(x|n)$ . The probability of observing  $x$  cells is then found by the number of ways of placing  $x$  cells into the neighborhood and the remaining  $n - x - 1$  (recall there are only  $n - 1$  since the focal one has already been placed) by

$$\mathbb{P}(x|n) = \frac{\binom{\omega}{x} \binom{l-\omega-1}{n-x-1}}{\binom{l-1}{n-1}}. \quad (3.8)$$

To solve for the bracketed term in (2.6), we are interested in the probability that all neighbor sites are occupied. For  $l, n \gg \omega$  this leads to

$$\mathbb{P}(\omega|n) = \left(\frac{n-1}{l-1}\right)^\omega \approx \left(\frac{n}{l}\right)^\omega, \quad (3.9)$$

we obtain

$$\dot{u} = \frac{1}{l} \lambda \left\langle \sum_{i=1}^n \left[ 1 - \left(\frac{n}{l}\right)^{\omega_i} \right] \right\rangle - \delta u. \quad (3.10)$$

To evaluate the sum, we consider a Taylor expansion up to second order about the mean  $\mu_\omega$  and 0. The first leads to

$$\dot{u} = \lambda u \left\{ 1 - u^{\mu_\omega} \left[ 1 + \frac{1}{2} \sigma_\omega^2 (\ln u)^2 \right] \right\} - \delta u. \quad (3.11)$$

Provided we can neglect the standard deviation ( $2 \gg (\sigma_\omega \ln u)^2$ ) we arrive at a generalized logistic differential equation,

$$\dot{u} = \lambda u (1 - u^{\mu_\omega}) - \delta u. \quad (3.12)$$

This particular form is identical to Richards' differential equation originally devised empirically as a flexible growth function which encompassed many growth laws (Richards, 1959).

If instead, we Taylor expand near 0, we obtain to second order

$$\dot{u} = -\lambda u \left[ \mu_\omega \ln u + \frac{1}{2} (\sigma_\omega^2 + \mu_\omega^2) (\ln u)^2 \right] - \delta u. \quad (3.13)$$

To neglect the higher order term imposes the condition

$$\frac{2\mu_\omega}{\sigma_\omega^2 + \mu_\omega^2} \gg |\ln u|. \quad (3.14)$$

This leads to

$$\dot{u} = -\lambda \mu_\omega u \ln u - \delta u, \quad (3.15)$$

which we recognize as a form of Gompertz's law. The ‘‘Gompertz condition’’ given by (3.14) provides some mathematical justification for why Gompertz fits are notoriously poor (and often incorrect) when the tumor is small. Modifications to these models to alleviate this issue have been introduced, an example is the Gompertz-Exponential model proposed by Wheldon, which assumes the tumor initially grows exponentially before switching to a Gompertz law (Wheldon, 1988). If we stipulate that Gompertz emerges via contact inhibition, then a necessary condition for this law to be valid is that  $u$  is not too small. This occurs through the  $\ln u$  term in (3.14), since a sufficient condition for this law to be a valid fit is if  $u \approx 1$  or if the mean number of neighbor sites ( $\mu_\omega$ ) is very small.

Interestingly, one does not recover logistic growth by assuming that every tumor cell can place offspring at each site. Indeed, (3.8) shows that when  $x = \omega$  and  $\omega = l - 1$

$$\mathbb{P}(l-1|n) = \frac{\binom{0}{n-l}}{\binom{l-1}{n-1}} = \begin{cases} 0 & \text{if } n < l \\ 1 & \text{if } n \geq l \end{cases} := I_{n \geq l}. \quad (3.16)$$

Here,  $I_{n \geq l}$  is an indicator function which is 1 when satisfied and 0 otherwise. This leads to the deterministic growth law

$$\dot{u} = \lambda u (1 - I_{u \geq 1}) - \delta u, \quad (3.17)$$

which implies exponential growth until saturation if  $\lambda > \delta$ .

### 3.4 Integrating the theory with experimental data

We fit the appropriate growth laws derived in the previous sections to experimental cell count measurements. For cells growing in a two-dimensional domain, we expected on average that the number of neighbor sites could range anywhere from 1 to 8. This parameter could be slightly lower overall due to a reduction near the boundary of the domain, but for sufficiently large domains relative to cell size, this reductive effect should be small. We calibrated Gompertz and generalized logistic growth laws using *NonlinearModelFit* (Wolfram Mathematica 12.0) with the temporal data obtained from the seven different cell lines for variable initial seeding conditions.

A prediction obtained from the derivation of Gompertz growth via contact inhibition was that the approximation to the mean-field growth law would be poor if the initial confluence was low. This effect has been noted both phenomenologically (Wheldon, 1988) and experimentally (Steel, 1977b). To test this, we compared relative goodness-of-fit between Gompertz and generalized logistic as a function of initial confluence for each cell line and each experimental setup (amount of initial confluence). An AIC score was obtained for both models and Gompertz's AIC score was normalized by the generalized logistic's AIC score. We plotted this normalized score against the initial confluence on a log-linear scale and fit a line using *LinearModelFit* (Wolfram Mathematica 12.0). The resulting fit and cell line data are plotted in Figure 4A. The dashed line at 1.0 is meant to guide the eye, values above this imply that Gompertz is improvement over generalized logistic. This is not to say that the fits are better, but more that no information is gained with generalized logistic, which carries an extra parameter. With an  $R_{\text{adj}}^2 = 0.24$ , the straight-line fit is not strong, but a general upward trend was observed as a function of initial confluence. We also plotted each cell line's individual fit (Figure 4A inset). The positive slope for each cell line indicates that Gompertz generally improves with higher initial confluence experiments.

Next, we fit the *in silico* experiments to the growth laws derived in the previous sections. For cells growing in a sufficiently large dish, we expect on average that the number of neighbor sites will be only weakly impacted by the boundary. This effect is slightly diminished due to the reduction near the boundary, but for sufficiently large systems relative to cell size the effect will be small. The derivation of Eq. (3.10) assumes that the probability of every site being occupied is independent of site location. A natural rule that justifies this assumption is if the movement of cells occurs at a much faster rate than cell cycle length. We further assume an inverse relationship exists between  $\lambda$  and  $\omega$  of the form  $C = \lambda\omega$ . This assumption is based on the results obtained from the fitting routine on the aggregate experimental data (Figure 4B).

We ran the ABM with  $\lambda\omega = 0.1$  and  $\delta = 0.001$ , and with the same fitting procedure as de-

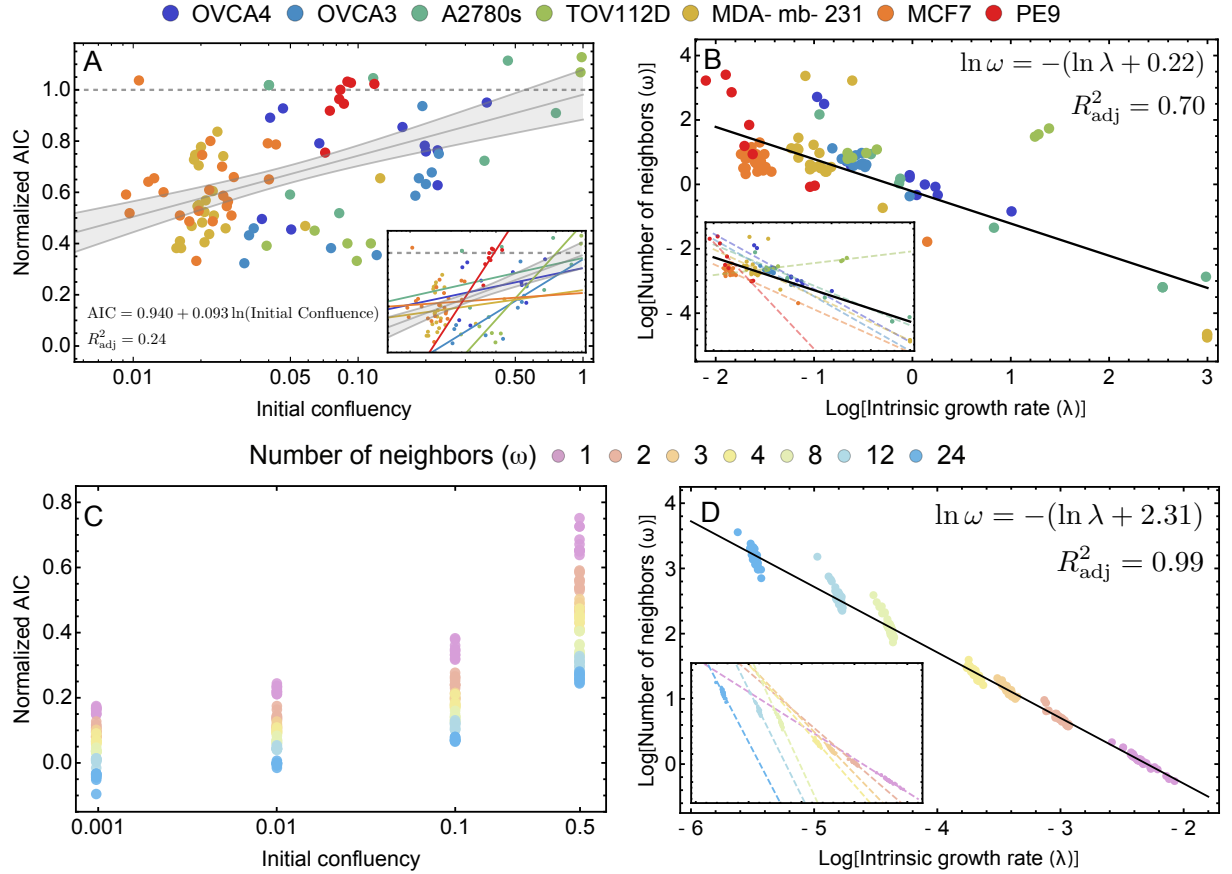


**Figure 4. Assessing model-fits for the different cell lines (given above) for *in vitro* and *in silico* ABM experiments, using an Akaike Information Criterion (AIC)** **A:** Confluency vs.  $AIC_{\text{Gompertz}}/AIC_{\text{Gen}}$ . Log. score, along with a best fit line that shows the general improvement of Gompertz fits as the initial confluency increases. **B:** Intrinsic growth rate vs. number of neighbors ( $\lambda, \omega$ ) on a log-log scale. Different experimental setups (initial confluence and cell line) are colored and a best fit line is determined. In Figures S1 and S2 we show individual fits using generalized logistic and Gompertz growth laws, respectively. **C:** Confluency vs.  $AIC_{\text{Gompertz}}/AIC_{\text{Gen}}$ . Log. score. **D:** ABM Intrinsic growth rate vs. Number of neighbors ( $\lambda, \omega$ ) on a log-log scale. Different birth neighborhood size are color coded and a best fit line is drawn.

scribed for the handling of the *in vitro* data. We then computed analogous statistics comparing goodness-of-fit, comparing growth rate vs. number of neighbors (Figure 4C-D). We found, as predicted, that higher initial confluency improves Gompertz’s goodness-of-fit (relative to generalized logistic) and that the fits also improve as  $\omega \rightarrow 0$ . However, the Gompertz-based procedure never reached the same goodness-of-fit as generalized logistic (compare this to Figure 4A). These differences in goodness-of-fit likely stem from the fact that it is difficult to give a natural rule to drive an ABM framework below a single cell as the birth neighborhood. Despite this discrepancy, the general trend of improvement of fit with increasing initial confluence and decreasing number of neighbors is consistent with the theoretical model.

We then looked at the relationship between growth rate and number of neighbors; using linear regression, we recaptured the growth law given to the ABM, by noting that if we take the log of both sides of  $\lambda\omega = 0.1$  and solve, we obtain  $\log \omega = -(\ln \lambda + 2.30)$  (see Figure 4D). However, we also observed an interesting trend within the groups defined by fixed birth neighborhood  $\omega$ . Instead of looking at the aggregate, if consider each value of  $\omega$  individually and use linear regression, the slopes appear to approach a value of -1, which implies an inverse-power law. Both the cell lines and *in silico* ABM simulations show a change in slope of the population surface growth, trending towards an inverse power law as  $\omega$  decreases. We discuss this relationship in detail in section 4.

## 4 Discussion

The emergence of multiple well-known tumor growth laws from the same individual based process via contact inhibition is striking. Given the prominence of cell-based models in cancer biology (Chamseddine and Rejniak, 2020; Metzcar et al., 2019), it is important to consider the implications of model construction on tumor growth dynamics. If we stipulate that a tumor’s primary impedance to divide is given by its inability to place offspring in a nearby location, than the mean-field (deterministic) law that determines the tumor growth is not necessarily unique. The fact that multiple growth laws can suffice to adequately model *in vitro* tumor growth can be attributed to the fact that these growth laws are approximations to the mean-field dynamics in different limits and when multiple laws are valid, we are at the intersection when these approximations all hold simultaneously.

The relationship between the parameters  $(\lambda, \omega, \delta)$  in the generalized logistic has interesting implications. Assuming an optimal pair with a small  $\omega$  has been obtained, one can travel along



this curve as  $\omega \rightarrow 0$ . The connection between Gompertz and generalized logistic is well known and requires  $\omega \rightarrow 0$  and  $r \rightarrow r_0/\omega$ , which implies that  $r\omega = r_0$  in the limit of small  $\omega$ . We thus fit the cell line data to this power law and obtained an adjusted  $R^2$  of 0.7. Looking at Figure 4B, it is clear that cell lines with a larger birth neighborhood size don't necessarily follow the same inverse-power law, but as  $\omega$  gets smaller the power seems to approach  $-1$ . Why do cell lines have different relationships between (average) birth neighborhood size  $\omega$  and net growth rate  $\lambda$ ? One explanation is surface area. Assuming a cell requires the ability to see an open area for division, a larger surface area would give it the ability to sense more open space. Thus, a natural prediction emerges from this theory. Cells with a large  $\omega$  are more likely to be irregularly shaped. In contrast, an argument can also be made for small  $\omega$  to point to cell shape irregularity, but from a non-optimal standpoint. A malleable shaped cell could easily see a time-dependent function of  $\omega$ . Alternatively, cell adhesion may have an impact on the number of allowed neighbor sites (Anderson, 2005).

Our model states that when a cell dies the site becomes open. Of note, necrosis is a well-documented phenomenon of growing tumors (Vakkila and Lotze, 2004). A necrotic core can form under hypoxic conditions. One can introduce a time scale on which a dead cell remains in place before being decomposed. During this time, the site would be inaccessible. A natural choice would be an exponential distribution with mean given by the time it takes for macrophages or other phagocytes to migrate to the location and engulf the dead cell. Of course, this introduction also implies that the immune system is a natural player in controlling the number of accessible sites for tumor cells to divide, both in their ability to remove debris (e.g. dead cells) and their physical occupation of space. Thus, a more controlled approach to model active cell removal could be a future addition to our model.

Cell-to-cell signaling is another possible extension that can be incorporated via a local dependency on  $\omega$ . These chemicals are often secreted in a paracrine fashion and lead to multiple cell interactions. These can promote or inhibit the ability for a cell to proliferate into new space. The inclusion of such factors can lead to a spatially-dependent  $\omega$  (or  $\lambda$ ), depending on where and how these factors are produced.

Fractal or radial growth demonstrates how the proper deterministic growth law can change over time. At low tumor volume, all cells are effectively surface dwelling cells. Hence, the dynamics of all radial/fractal growing tumors are initially exponential. The shift from exponential to fractal depends on the birth neighborhood size. Unless the birth neighborhood size is all sites  $\omega_i = l$ , the tumor will begin to transition from exponential to fractal-like growth, which can be most easily seen when tumor growth is presented on a log-log scale. As the tumor continues to grow,

the fractal dimension approaches  $d - 1$ . A possible explanation for this is to first recognize that no tumor growth is purely fractal as there is a minimal length scale. As the tumor gets larger, the local curvature will begin to flatten relative to the size of the overall tumor and begin to look more and more symmetric. Alternatively, one can view this as shifting your viewpoint further and further from a tumor, it will begin to look more regular.

In summary, our theory offers a possible explanation for the large number of mean-field laws that can adequately capture tumor growth dynamics. We do so through unification under density-dependent birth events via contact inhibition. Of note, we present the first mechanistic derivation of Gompertzian growth based on contact inhibition.

## References

- A. Aguilera and B. Gómez-González. Genome instability: a mechanistic view of its causes and consequences. *Nature Reviews Genetics*, 9(3):204–217, 2008.
- P. M. Altrock, L. L. Liu, and F. Michor. The mathematics of cancer: integrating quantitative models. *Nature Reviews Cancer*, 15:730–745, 2015.
- A. R. Anderson. A hybrid mathematical model of solid tumour invasion: the importance of cell adhesion. *Mathematical medicine and biology: a journal of the IMA*, 22(2):163–186, 2005.
- S. Benzekry, C. Lamont, A. Beheshti, A. Tracz, J. M. Ebos, L. Hlatky, and P. Hahnfeldt. Classical mathematical models for description and prediction of experimental tumor growth. *PLoS Comput Biol*, 10(8):e1003800, 2014.
- R. Brady and H. Enderling. Mathematical models of cancer: when to predict novel therapies, and when not to. *Bulletin of mathematical biology*, 81(10):3722–3731, 2019.
- R. R. Bravo, E. Baratchart, J. West, R. O. Schenck, A. K. Miller, J. Gallaher, C. D. Gatenbee, D. Basanta, M. Robertson-Tessi, and A. R. Anderson. Hybrid automata library: A flexible platform for hybrid modeling with real-time visualization. *PLoS Computational Biology*, 16(3):e1007635, 2020.
- I. M. Chamseddine and K. A. Rejniak. Hybrid modeling frameworks of tumor development and treatment. *Wiley Interdisciplinary Reviews: Systems Biology and Medicine*, 12(1):e1461, 2020.
- G. Cheng, J. Tse, R. K. Jain, and L. L. Munn. Micro-environmental mechanical stress controls tumor spheroid size and morphology by suppressing proliferation and inducing apoptosis in cancer cells. *PLoS one*, 4(2):e4632, 2009.
- H. Eagle and E. M. Levine. Growth regulatory effects of cellular interaction. *Nature*, 213(5081):1102–1106, 1967.

- J. Gallaher and A. R. Anderson. Evolution of intratumoral phenotypic heterogeneity: the role of trait inheritance. *Interface focus*, 3(4):20130016, 2013.
- P. Gerlee. The model muddle: in search of tumor growth laws. *Cancer research*, 73(8):2407–2411, 2013.
- C. Guiot, P. G. Degiorgis, P. P. Delsanto, P. Gabriele, and T. S. Deisboeck. Does tumor growth follow a "universal law"? *Journal of Theoretical Biology*, 225(2):147–151, 2003.
- H. Hatzikirou, D. Basanta, M. Simon, K. Schaller, and A. Deutsch. ‘go or grow’: the key to the emergence of invasion in tumour progression? *Mathematical medicine and biology: a journal of the IMA*, 29(1):49–65, 2012.
- J. Hausser and U. Alon. Tumour heterogeneity and the evolutionary trade-offs of cancer. *Nature Reviews Cancer*, 20(4):247–257, 2020.
- T. Islam, D. G. Fiebig, and N. Meade. Modelling multinational telecommunications demand with limited data. *International Journal of Forecasting*, 18(4):605–624, 2002.
- G. J. Kimmel, M. Dane, L. M. Heiser, P. M. Altrock, and N. Andor. Integrating mathematical modeling with high-throughput imaging explains how polyploid populations behave in nutrient-sparse environments. *Cancer Research*, 80(22):5109–5120, 2020.
- G. J. Kimmel, F. L. Locke, and P. M. Altrock. The roles of T cell competition and stochastic extinction events in chimeric antigen receptor t cell therapy. *Proceedings of the Royal Society B*, 288(1947):20210229, 2021.
- A. Laird. Dynamics of tumour growth. *British Journal of Cancer*, 18(3):490, 1964.
- R. Mayor and C. Carmona-Fontaine. Keeping in touch with contact inhibition of locomotion. *Trends in Cell Biology*, 20(6):319–328, 2010.
- A. I. McClatchey and A. S. Yap. Contact inhibition (of proliferation) redux. *Current Opinion in Cell Biology*, 24(5):685–694, 2012.
- J. Metzcar, Y. Wang, R. Heiland, and P. Macklin. A review of cell-based computational modeling in cancer biology. *JCO Clinical Cancer Informatics*, 2:1–13, 2019.
- J. C. Mombach, N. Lemke, B. E. Bodmann, and M. A. P. Idiart. A mean-field theory of cellular growth. *EPL (Europhysics Letters)*, 59(6):923, 2002.
- R. Orbach. Dynamics of fractal networks. *Science*, 231(4740):814–819, 1986.
- M. Pavel, M. Renna, S. J. Park, F. M. Menzies, T. Ricketts, J. Füllgrabe, A. Ashkenazi, R. A. Frake, A. C. Lombarte, C. F. Bento, et al. Contact inhibition controls cell survival and proliferation via yap/taz-autophagy axis. *Nature Communications*, 9(1):1–18, 2018.
- V. M. Pérez-García, G. F. Calvo, J. J. Bosque, O. León-Triana, J. Jiménez, J. Pérez-Beteta, J. Belmonte-Beitia, M. Valiente, L. Zhu, P. García-Gómez, et al. Universal scaling laws rule explosive growth in human cancers. *Nature Physics*, pages 1–6, 2020.

- J. G. Reiter, M. Baretta, J. M. Gerold, A. P. Makohon-Moore, A. Daud, C. A. Iacobuzio-Donahue, N. S. Azad, K. W. Kinzler, M. A. Nowak, and B. Vogelstein. An analysis of genetic heterogeneity in untreated cancers. *Nature Reviews Cancer*, 19(11):639–650, 2019.
- D. Ribatti. A revisited concept: Contact inhibition of growth. from cell biology to malignancy. *Experimental Cell Research*, 359(1):17–19, 2017.
- F. Richards. A flexible growth function for empirical use. *Journal of Experimental Botany*, 10(2):290–301, 1959.
- I. A. Rodriguez-Brenes, N. L. Komarova, and D. Wodarz. Tumor growth dynamics: insights into evolutionary processes. *Trends in Ecology and Evolution*, 28(10):597–604, 2013.
- J. A. Spratt, D. Von Fournier, J. S. Spratt, and E. E. Weber. Decelerating growth and human breast cancer. *Cancer*, 71(6):2013–2019, 1993.
- G. Steel. Growth kinetics of tumors. *Cell population kinetics in relation to the growth and treatment of cancer*, pages 59–61, 1977a.
- G. G. Steel. Growth kinetics of tumors. *Cell population kinetics in relation to the growth and treatment of cancer*, pages 59–61, 1977b.
- J. Vakkila and M. T. Lotze. Inflammation and necrosis promote tumour growth. *Nature Reviews Immunology*, 4(8):641–648, 2004.
- S. T. Vittadello, S. W. McCue, G. Gunasingh, N. K. Haass, and M. J. Simpson. Examining go-or-grow using fluorescent cell-cycle indicators and cell-cycle-inhibiting drugs. *Biophysical Journal*, 2020.
- J. West and P. Newton. Cellular interactions constrain tumor growth. *Proceedings of the National Academy of Sciences*, 116(6):1918–1923, 2019. ISSN 0027-8424. doi: 10.1073/pnas.1804150116.
- J. West, Z. Hasnain, P. Macklin, and P. K. Newton. An evolutionary model of tumor cell kinetics and the emergence of molecular heterogeneity driving gompertzian growth. *SIAM Review*, 58(4):716–736, 2016.
- T. E. Wheldon. *Mathematical models in cancer research*. Taylor & Francis, 1988.
- D. Wodarz and N. Komarova. *Computational biology of cancer: Lecture notes and mathematical modeling*. World Scientific Publishing, 2005.
- M. Zwietering, I. Jongenburger, F. Rombouts, and K. Van’t Riet. Modeling of the bacterial growth curve. *Applied and Environmental Microbiology*, 56(6):1875–1881, 1990.

## Supplementary Materials

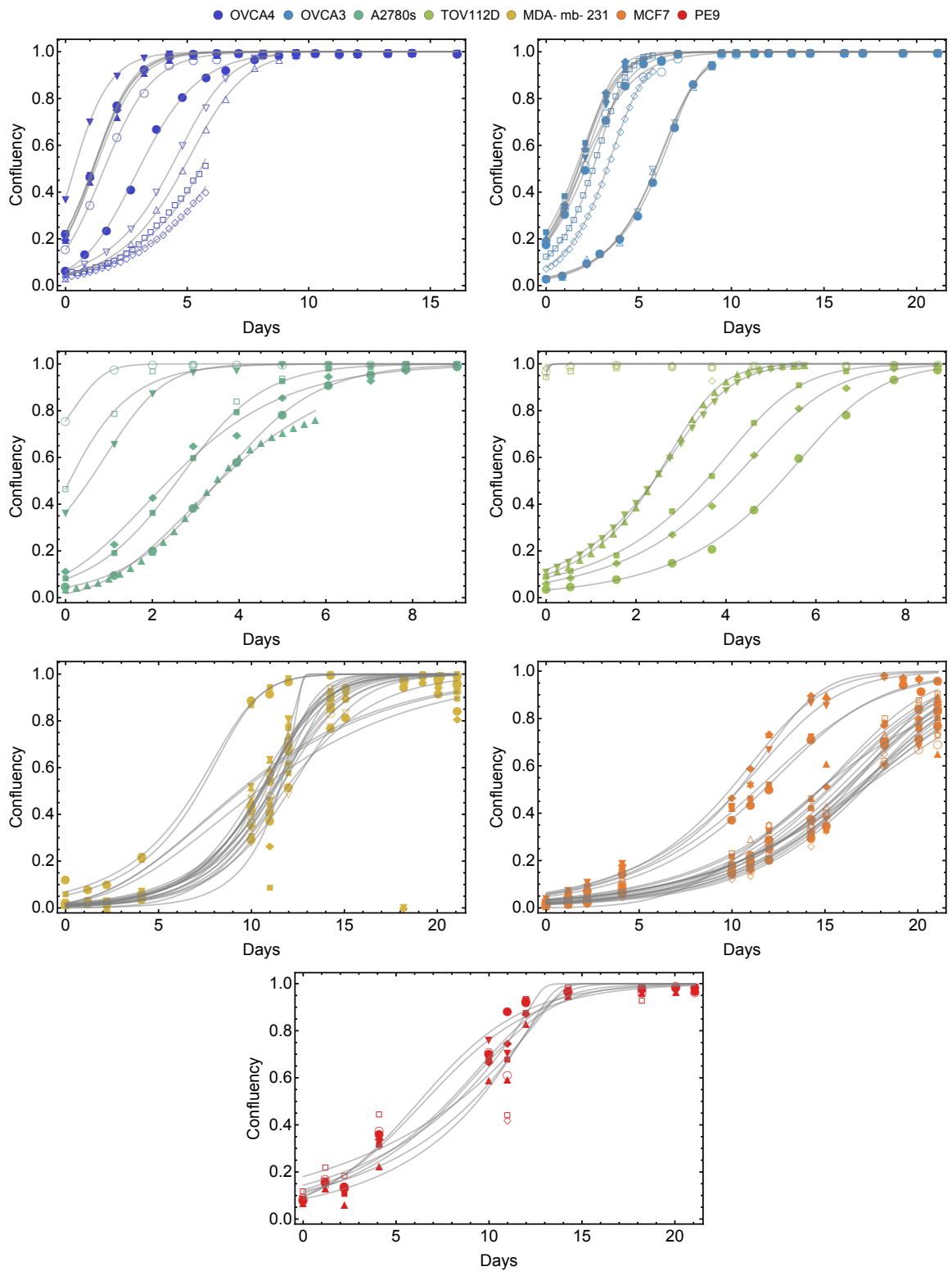


Figure S1. Fitting a generalized logistic growth law of longitudinal *in vitro* growth data of the the seven cell lines (see Methods).

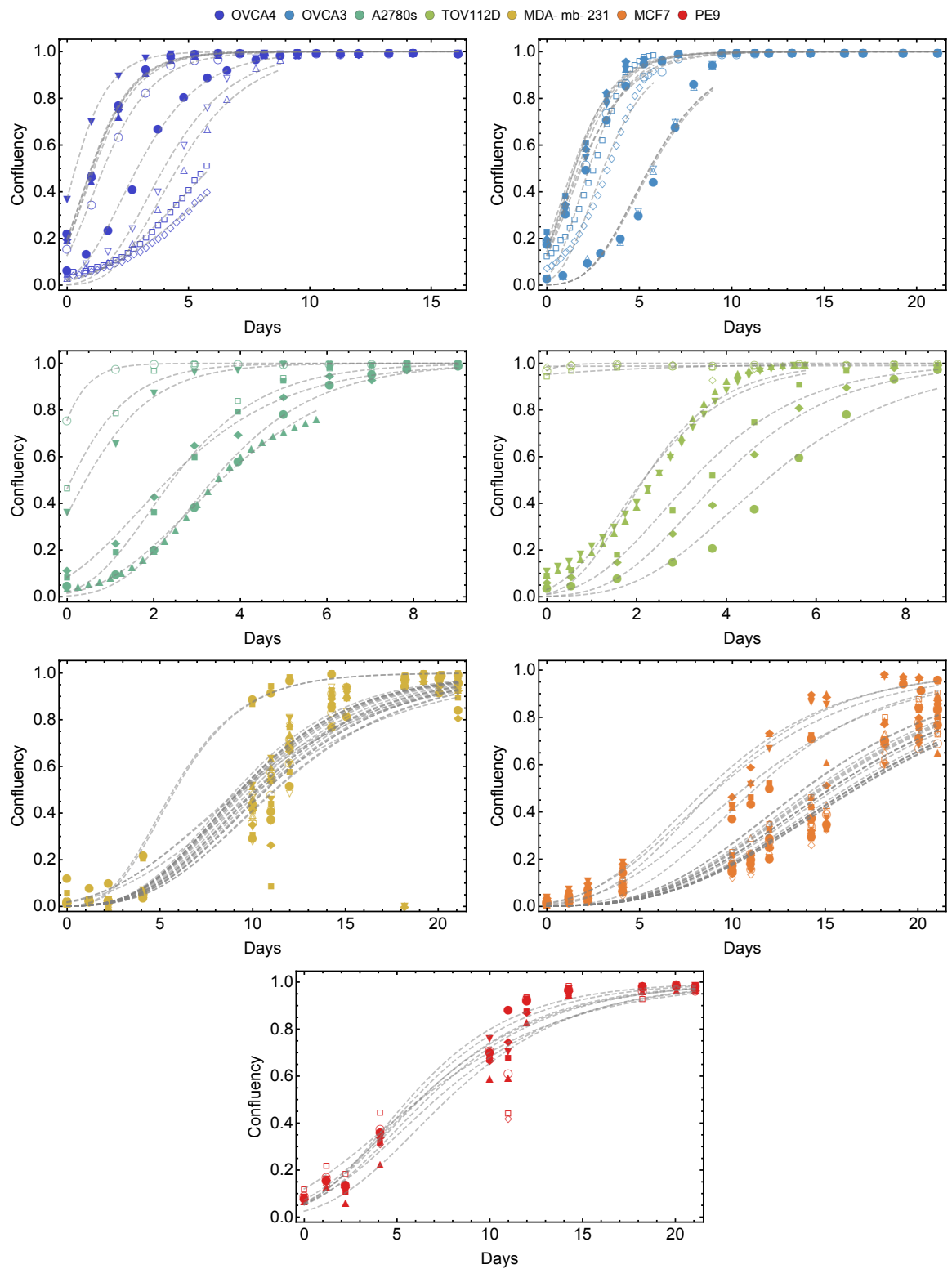


Figure S2. Fitting a Gompertz growth law of longitudinal *in vitro* growth data of the the seven cell lines (see Methods).